

# A general multi-modal data learning method for Person Re-identification

Gong Yunpeng

College of Mathematics and Information, Fujian Normal University  
{fmonkey625}@gmail.com

**Abstract.** This paper proposes a general multi-modal data learning method, which includes Global Homogeneous Transformation, Local Homogeneous Transformation and their combination. During ReID model training, on the one hand, it randomly selected a rectangular area in the RGB image and replace its color with the same rectangular area in corresponding homogeneous image, thus it generate a training image with different homogeneous areas; On the other hand, it convert an image into a homogeneous image. These two methods help the model to directly learn the relationship between different modalities in the Special ReID task. In single-modal ReID tasks, it can be used as an effective data augmentation. The experimental results show that our method achieves a performance improvement of up to 3.3% in single modal ReID task, and performance improvement in the Sketch Re-identification more than 8%. In addition, our experiments also show that this method is also very useful in adversarial training for adversarial defense. It can help the model learn faster and better from adversarial examples. The code is available at <https://github.com/finger-monkey/Data-Augmentation>.

**Keywords:** Person Re-identification, Data Augmentation, Global Homogeneous Transformation, Local Homogeneous Transformation, Sketch re-identification, Adversarial Training

## 1 Introduction

Person Re-identification (ReID) is usually viewed as an image retrieval matter, which aims to perform cross-camera retrieval of pedestrians to determine whether a particular pedestrian shows up in the image or video sequence taken by a camera. The challenge of this task is that the images taken by different cameras often contain significant intra-class changes caused by changes in perspective, human posture, light changes, occlusion, etc., that is, the appearance of the same pedestrian image may change greatly, so that the intra class (the same pedestrian) difference between pedestrians may be greater than the inter class (different pedestrians) difference.

Therefore, finding more robust features and measurement methods to effectively solve the above problems has become one of the main goals of pedestrian re-identification. The pipeline of ReID model As shown in the Fig.1.

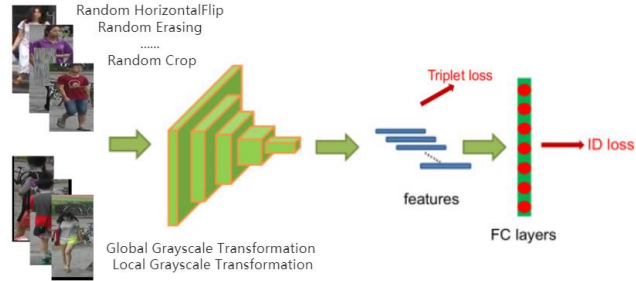


**Fig. 1.** The pipeline of ReID model

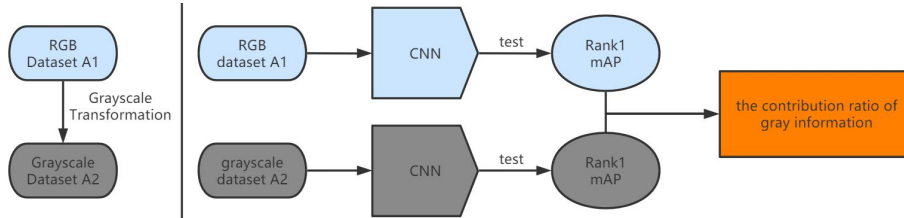
ReID research articles published in recent years show that the generalization ability of ReID models is closely related to the training method of the models. For example, Luo, Liao et al. use many training tricks to effectively improve the performance of the model [1]. Liao proposed fastReID which used more training tricks [2], this method surpassed the highest performance of CVPR2020 model [4].

Fig.2 shows that images are most susceptible to lighting changes and lose more color information in environments of pedestrians replacing clothes and low resolution, but they have the same spatial structure. This variety is common in many datasets. A grayscale image is an RGB image which loses some color information but retains its spatial structure. In human cognition, humans can recognize different objects through grayscale images. Therefore, it is an important issue how to use spatial structural information to reduce the adverse impact of illumination changes on ReID.



**Fig. 2.** Left: The first line are RGB images, the second line are the corresponding grayscale images. The images from left to right are: normal images with sharp contrast, low contrast dress, dark and gray dress, and blurred or low resolution images due to the movement of pedestrians (the images in the dataset are themselves of lower resolution). Right: Images of a pedestrian in different dresses, generated by GAN.

To show the importance of grayscale information for ReID query task, we designed the following experiments: dataset A1 is composed of RGB images, dataset A2 is composed of homogeneous grayscale images which is transformed by RGB images, A1 and A2 are trained and tested on the same model respectively, the ratio of the corresponding performance of the model on A1 and A2 is regarded as the contribution rate of grayscale information, as shown in Fig.3.



**Fig. 3.** The illustration is a schematic diagram of the experiment on the grayscale contribution.

Tested on three datasets, the contribution of grayscale images is shown in Tab.1.

**Table 1.** Contribution rate of grayscale information on MSMT17, DukeMTMC, and Market-1501 for the ReID.

Dataset	Rank-1	Rank-5	Rank-10	mAP
Market1501[13]	89.3%	95.4%	97.5%	73.4%
DukeMTMC[14]	91.0%	94.1%	95.2%	77.7%
MSMT17[16]	87.1%	91.7%	99.8%	70.6%

The experimental results show that grayscale images contribute more than 80% - 90% to the retrieval accuracy. More importantly, the contribution of grayscale images to the retrieval accuracy in Rank-10 is more than 95%. This result indicates that the spatial structure information of grayscale images has great potential for the ReID retrieval. Meanwhile, Zheng et al. used the generative adversarial network to change the clothes color of pedestrian in the image and generate more diverse data. This trick improves the ReID model's generalization ability [8], as is shown in the right column of Fig.2. Inspired by Zheng, we assume that homogeneous grayscale images of RGB images can also achieve the same goal of improving model performance, and can effectively reduce the impact of color variation produced by low contrast, the blurred images or low resolution images resulting from the movement of the pedestrians or changes in lighting.

Based on the above analysis, in single-modal ReID tasks, our method can be used as an effective data augmentation by introducing grayscale information. In this case, we call the proposed method grayscale data augmentation method to improve the model performance. Grayscale Data Augmentation has the following advantages:

(1) It is a lightweight approach which does not require any additional parameter learning or memory consumption. It can be combined with various CNN models without changing the learning strategy.

(2) It is a complementary approach to existing data augmentation. When these methods are used altogether, Grayscale Data Augmentation can further improve model performance.

Our main contributions are summarized as follows:

(1) An effective grayscale data augmentation method is proposed to make full use of the structural information of grayscale images, which effectively minimizes adverse impact of illumination variation.

(2) We have conducted a large number of experiments on three ReID datasets and analyzed the experimental results, which demonstrates effectiveness of the proposed method.

The multi-modal data learning methods we proposed basically have the above advantages. Below we mainly explain related work and our method from the perspective of Grayscale Data Augmentation.

## 2 Related Work

Since deep learning was introduced into ReID field, many ReID methods have been proposed. An active field in ReID research is to utilize GANs to augment training data. For example, Zheng et al. used generative adversarial networks to replace the clothing of each pedestrian with the clothes of other pedestrians, so as to generate more diversified data to reduce the dependence of the model on color information and improve the generalization ability of the model [8]. In addition, some recent studies also employ some effective training tricks to improve the generalization ability of the model. For example, Luo et al. evaluate these effective training tricks in [1]. It's well known that data augmentation such as Random Cropping and Random Flipping plays an important role in the field of classification, detection and ReID, all of them increase the diversity of training data, and improve the generalization ability of the model to some extent. The Random Erasing proposed by Zhong et al. [3] simulates the occlusion problem that is frequently encountered in reality, which randomly erases a part of the image with a certain probability in the training samples to increase the diversity of the training samples. To some extent, it resolves the problems of inadequate generalization ability when the recognition task faces the occlusion problem, so it has become an effective training trick in the field of ReID. Fan et al. found that the learning rate has a great impact on the performance of a ReID model, a warmup strategy used is applied to bootstrap the network for better performance [5]. Label smoothing proposed is a widely used method to prevent overfitting for a classification task [6]. The k-reciprocal encoding is used to reorder the results of the query to improve mAP and Rank-1 [7]. This trick is known as re-Rank. The homogeneity of softmax loss and triplet loss functions was pointed out by Circle Loss, and a new loss to unify these two paradigms is proposed, the best ReID performance is achieved on Market-1501 dataset [15]. Although these methods are different, they improve the generalization ability of the ReID model from different perspectives and aspects. This encourages us to open our minds and look for ways to solve problems from more perspectives.

### 3 The Proposed Approach

Given the fact that the structural information of grayscale images has a great impact on the performance of ReID, our method can be used as an effective data augmentation to take full advantage of the grayscale structural information and fit the color of RGB images. In this case, we call the proposed method: Grayscale Data Augmentation, which includes Global Grayscale Transformation(GGT), Local Grayscale Transformation(LGT), and their combination. The framework of the proposed method is shown in Fig.4 and Fig.5.

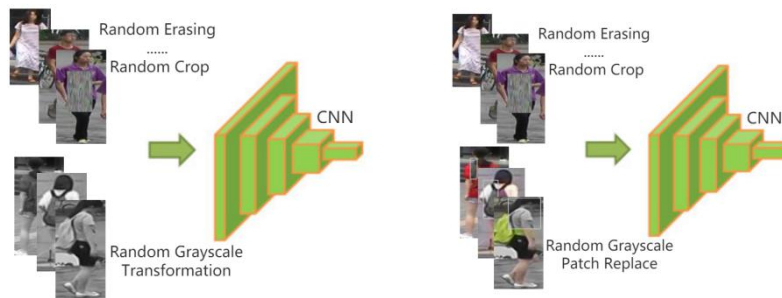


Fig. 4. Application of GGT(left) and LGT(right) in pipelines of the baseline.



Fig. 5. Schematic diagram of Local Grayscale Transformation.

#### 3.1 Global Grayscale Transformation (GGT)

In order to diversify the data and preserve the spatial structure information of the RGB images, before training samples are input into neural network, we conduct GGT randomly transformation on the entire batch of training images with a certain probability. A grayscale image is generated by performing a pixel-by-pixel linear cumulative transformation on the R, G, B channels of the original RGB image. The procedure of GGT is shown in algorithm1.

---

**Algorithm1 : Global Grayscale Transformation Procedure**

---

---

**Input :** Input batch RGB images  $I$ ;  
**Gray transformation probability  $p$ ;**  
**Output:** mini-batch of grayscale images  $I^*$  .

- 1 **Initialization:**  $p_1 \leftarrow \text{Rand}(0, 1)$ .
- 2 **if**  $p_1 \geq p$  **then**
- 3      $I^* \leftarrow I$ ;
- 4     **return**  $I^*$  .
- 5 **End**

---

### 3.2 Local Grayscale Transformation (LGT)

In the process of model training, we conduct LGT randomly transformation on the entire batch of training images with a certain probability. For an image  $I$  in a mini-batch, denote the probability of it undergoing LGT be  $p$ , and the probability of it being kept unchanged be  $1-p$ . In this process, it randomly selects a rectangular region in the image and replaces it with the pixels of the same rectangular region in the corresponding grayscale image. Thus, training images which include regions with different levels of grayscale are generated. Among them,  $s_l$  and  $s_h$  are the minimum and maximum values of the ratio of the image to the randomly generated rectangle area, and the  $S_e$  of the rectangle area limited between the minimum and maximum ratio is obtained by  $S_e \leftarrow \text{Rand}(s_l, s_h) \times S$ ,  $r_e$  is a coefficient used to determine the shape of the rectangle. It is limited to the interval  $(r_1, r_2)$ .  $x_e$  and  $y_e$  are randomly generated by coordinates of the upper left corner of the rectangle. If the coordinates of the rectangle exceed the scope of the image, the area and position coordinates of the rectangle are re-determined. When a rectangle that meets the above requirements is found, the pixel values of the selected region are replaced by the corresponding rectangular region on the grayscale image converted from RGB image. As a result, training images which include regions with different levels of grayscale are generated, and the object structure is not damaged. The procedure of LGT is shown in Algorithm.2.

---

**Algorithm 2: Local Grayscale Transformation Procedure**

---

---

```

Input: Input image I;
         Image size W and H;
         Area of image S;
         Erasing probability  $p_r$ ;
         Erasing area ratio range  $s_1$  and  $s_h$  ;
         Erasing aspect ratio range  $r_1$  and  $r_2$  .

Output: Grayscale erased image  $I^*$  .

1 Initialization:  $p_1 \leftarrow \text{Rand}(0, 1)$ .
2 if  $p_1 \geq p_r$  then
3   |  $I^* \leftarrow I$ ;
4   | return  $I^*$  .
5 else
6   | while True do
7     |  $S_e \leftarrow \text{Rand}(s_1, s_h) \times S$ ;
8     |  $r_e \leftarrow \text{Rand}(r_1, r_2)$ ;
9     |  $H_e \leftarrow \text{Sqrt}(S_e \times r_e)$ ,  $W_e \leftarrow \text{Sqrt}(S_e / r_e)$ ;
10    |  $x_e \leftarrow \text{Rand}(0, W)$ ,  $y_e \leftarrow \text{Rand}(0, H)$ ;
11    | if  $x_e + W_e \leq W$  and  $y_e + H_e \leq H$  then
12      |  $I_e \leftarrow (x_e, y_e, x_e + W_e, y_e + H_e)$ ;
13      |  $I(I_e) \leftarrow \text{Grayscale}(I_e)$ ;
14      |  $I^* \leftarrow I$ ;
15      | return  $I^*$ 
16    | end
17 end
18

```

---

## 4 Comparison and Analysis

In this section we will compare the performance of our approach with state-of-the-art methods on three baselines. The baselines are the ReID\_baseline[10], the strong baseline [1] and FastReID[2]. Since the model requires more training epochs to fit than the original, we add 0.5-1.5 times more training epochs to the training process.

### 4.1 Datasets

We conducted comparison experiments on MTMC17[16], DukeMTMC[14], and Market-1501[13].

The MSMT17 dataset, created in winter, was presented in 2018 as a new, larger dataset closer to real-life scenes, containing a total of 4,101 individuals and covering multiple scenes and time periods.

The DukeMTMC is a large-scale Multi-Target, Multi-Camera (MTMC) tracking dataset, a HD video dataset recorded by 8 synchronous cameras, with more than 7,000 single camera tracks and more than 2,700 individual pedestrians.

The Market-1501 dataset was collected in the summer of 2015. It includes 1,501 pedestrians captured by six cameras (five HD cameras and one low-definition camera).

These three datasets are currently the largest datasets of ReID, and they are also the most representative because they collectively contain multi-season, multi-time, HD, and low-definition cameras with rich scenes and backgrounds as well as complex lighting variations.

We evaluated these three datasets using Rank-k precision and mean Average Precision(mAP). Rank-1 denotes the average accuracy of the first returned result corresponding to each query image; mAP denotes the mean of average accuracy, the query results are sorted according to the similarity, the closer the correct result is to the top of the list, the higher the score.

## 4.2 Hyper-Parameter Setting

During CNN training, two hyper-parameters need to be evaluated. One of them is RGT probability  $p$ . Firstly, we take the hyper-parameter  $p$  as 0.01, 0.03, 0.05, 0.07, 0.1, 0.2, 0.3, ..., 1 for the RGT experiments. Then we take the value of each parameter for three independent repetitions of the experiments. Finally, we calculate the average of the final result. The results of different  $p$  are shown in Fig.6.

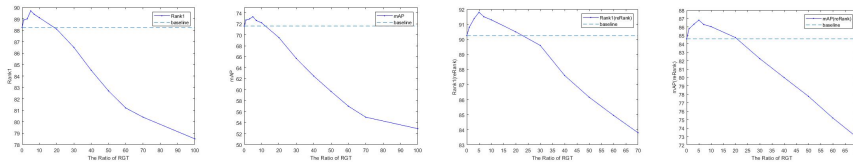


Fig. 6. Accuracy under different hyper-parameters on Market-1501 using baseline[10].

We can see that when  $p=0.05$ , the performance of the model reaches the maximum value in Rank-1 and mAP in Fig.7. If we do not specify, the hyper-parameter is set  $p=0.05$  in the next experiments.

Another hyper-parameter is RGPR probability  $p_r$ . We take the hyper-parameter  $p_r$  as 0.01, 0.03, 0.05, 0.07, 0.1, 0.2, 0.3, ..., 1 for the RGPR experiments, whose selection process is similar to the above  $p$ . The results of different  $p_r$  are shown in Fig.7.

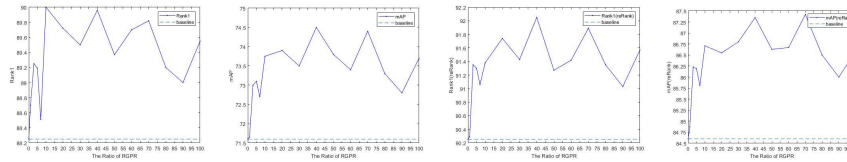


Fig. 7. Accuracy under different hyper-parameters on Market-1501 using baseline[10].



Obviously, when  $p_r=0.4$  or  $p_r=0.7$ , the model achieves better performance. And the best performance is achieved when  $p_r=0.4$ . If we do not specify, the hyper-parameter is set  $p_r=0.4$  in the later experiments.

### 4.3 Effectiveness of GGT and LGT

**Evaluation of GGT and LGT.** Compared with the best results of GGT on baseline [10], the accuracy of LGT is improved by 0.5% and 1.4% on Rank-1 and mAP, respectively. Under the same conditions using re-Rank, the accuracy of Rank-1 and mAP is improved by 0% and 0.4%, respectively. Therefore, the advantages of LGT are more obvious when re-Rank is not used. However, Fig.8 also shows that the performance improvement brought by LGT is not stable enough because of the obvious fluctuation in LGT, while the performance improvement brought by GGT is very stable. Therefore, we improve the stability of the method by combining GGT with LGT.

**Evaluation by Combining GGT with LGT.** First, we fix the hyper-parameter value of GGT to  $p=0.05$ , then keep the control variable unchanged to further determine the hyper-parameter of LGT. Finally, we take the hyper-parameter  $p_r$  of RGPR to be 0.1, 0.2, ..., 0.7 to conduct combination experiments of GGT and LGT, and conduct 3 independent repeated experiments for each parameter  $p_r$  to get the average value. The result is shown in Fig.8:

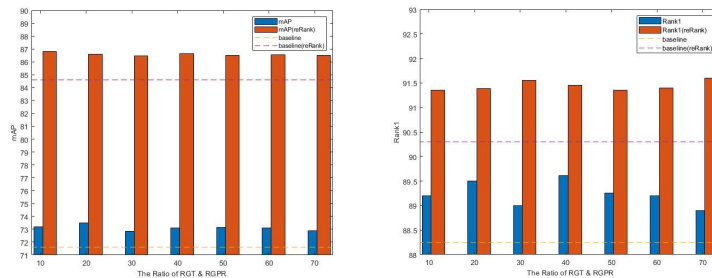


Fig. 8. Model performance of combining GGT with LGT.

It can be seen from Fig.8 that the performance improvement brought by the combination of GGT and LGT is more stable and with less fluctuation, and the comprehensive performance of the model is the best when the hyper-parameter value of LGT is  $p_r=0.4$ .

### 4.4 Performance Comparison and Analysis

We first evaluate each baseline on the Market-1501 dataset. Our method improves by 1.2% on Rank-1 and 3.3% on mAP on ReID\_baseline [10], and 1.5% on Rank-1 and 2.1% on mAP above baseline in the same conditions using the re-Rank. The best results of our method improve by 0.6% and 1.3% on the Rank-1 and mAP on the strong baseline [1], respectively, and 0.8% and 0.5% Rank-1 and mAP above

baseline under the same conditions using the re-Rank, respectively. On fastReID [2], our method is 0.2% higher and 0.9% than baseline in Rank-1 and mAP, respectively, and higher 0.1% and 0.3% than baseline under using re-Rank.

A comparison of the performance of our method with the state-of-the-art methods in three datasets is shown in Table 2 and Table 3.

**Table 2.** Performance comparison on MTMC17 datasets.

Methods	MTMC17	
	Rank-1	mAP
IANet[25] (CVPR'19)	75.5	46.8
DGNet[8](CVPR'19)	77.2	52.3
OSNet[9](ICCV'19)	78.7	52.9
BAT-net[11](ICCV'19)	79.5	56.8
RGA-SC[19](CVPR'20)	80.3	57.5
SCSN[18](CVPR'20)	83.8	58.5
AdaptiveReID[17](arXiv'20)	81.7	62.2
fastReID[2]	85.1	63.3
fastReID + GGT(ours)	<b>86.2</b>	<b>65.3</b>
fastReID + GGT&LGT(ours)	<b>86.2</b>	<b>65.9</b>

**Table 3.** Performance comparison on DukeMTMC、Market-1501 datasets.

Methods	Market1501		DukeMTMC	
	Rank-1	mAP	Rank-1	mAP
PCB [20] (ECCV'18)	92.3	77.4	81.8	66.1
AANet [24] (CVPR'19)	93.9	83.4	87.7	74.3
IANet [25] (CVPR'19)	94.4	83.1	87.1	73.4
Auto-ReID [28] (ICCV'19)	94.5	85.1	—	—
DG-Net[8](CVPR'19)	94.8	86.0	86.6	74.8
Pyramid [26] (CVPR'19)	95.7	88.2	89.0	79.0
ABDNet [27] (ICCV'19)	95.6	88.3	89.0	78.6
SONA [22] (ICCV'19)	95.7	88.7	89.3	78.1
SCAL [23] (ICCV'19)	95.8	89.3	89.0	79.6
CAR [21] (ICCV'19)	96.1	84.7	86.3	73.1
Circle Loss [15] (CVPR'20)	96.1	87.4	89.0	79.6
ReID_baseline[10]	88.8	71.6	—	—
ReID_baseline + reRank	90.5	85.2	—	—
ReID_baseline + GGT(ours)	<b>89.5</b>	<b>73.5</b>	—	—
ReID_baseline + GGT+ reRank(ours)	<b>92.0</b>	<b>86.9</b>	—	—
ReID_baseline + LGT(ours)	<b>90.0</b>	<b>74.9</b>	—	—
ReID_baseline + LGT+ reRank(ours)	<b>92.0</b>	<b>87.4</b>	—	—
strong baseline[1]	94.5	85.9	86.4	76.4
strong baseline + reRank	95.4	94.2	90.3	89.1
strong baseline + GGT(ours)	<b>94.6</b>	85.7	<b>87.8</b>	<b>77.3</b>
strong baseline + GGT+ reRank(ours)	<b>96.2</b>	<b>94.7</b>	<b>90.9</b>	<b>89.2</b>
strong baseline + LGT(ours)	<b>95.1</b>	<b>87.2</b>	<b>87.3</b>	<b>77.3</b>

strong baseline + LGT+ reRank(ours)	<b>95.9</b>	<b>94.4</b>	<b>91</b>	<b>89.4</b>
fastReID[2]	96.3	90.3	92.4	83.2
fastReID + reRank	96.8	95.3	94.4	92.2
fastReID + GGT(ours)	<b>96.5</b>	<b>91.2</b>	92.5	83.8
fastReID + GGT + reRank(ours)	<b>96.9</b>	<b>95.6</b>	94.4	92.5
fastReID + LGT(ours)	96.4	90.9	<b>92.8</b>	<b>84.2</b>
fastReID + LGT+ reRank(ours)	96.6	95.2	94.3	<b>92.7</b>

Next we evaluate each baseline on DukeMTMC dataset, the best results of our method on the strong baseline [1] improved by 1.4% on Rank-1, 0.9% on mAP, respectively, and 0.7% on Rank-1, 0.3% on mAP using the re-Rank, respectively. Our method on fast-ReID[2] improves by 0.4% and 1% on Rank-1 and mAP, respectively, and higher 0.5% on mAP than baseline under using the re-Rank.

Finally, we evaluate each baseline on the MTMC17 dataset, the best results of our method on fastReID[2] improve by 1.1% and 2.6% over baseline on Rank-1 and mAP, respectively.

To our knowledge, applying our approach to fastReID, we have achieved the highest retrieval accuracy currently available on the MTMC17 and Market-1501 datasets.

On the one hand, our method achieves better ReID performance because of exploiting the grayscale transformation, which increases the number and diversity of training samples. On the other hand, exploiting the structural information retained by the grayscale image, the colors of the RGB images and the spatial structural information of the grayscale images are fitted to each other in the model training, reducing the adverse effects of illumination variations on ReID.

## 5 Sketch Re-identification

In this section we will compare the performance of our approach with state-of-the-art methods on sketch Re-ID dataset.

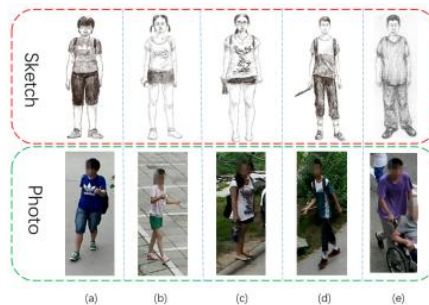


**Fig. 9.** Challenges of sketch Re-ID. Sketches lack color information and contain person's outline information. (a-b) Photos are affected by camera viewpoint. (b-c) Human pose is various. (c-d) Photos are full of cluttered background. (e) Person is occluded.

## 5.1 Datasets

sketch ReID dataset[31] contains 200 persons, each of which has one sketch and two photos. Photos of each person were captured during daytime by two cross-view cameras. It cropped the raw images (or video frames) manually to make sure that every photo contains the one specific person. It have a total of 5 artists to draw all persons' sketches and every artist has his own painting style.



**Fig. 10.** The first image is the result of Global Sketch Transformation(GST), the rest of images are the result of Local Sketch Transformation(LST).

## 5.2 Proposed Approach and Experiments

Through the application of the proposed Global Homogeneity Transformation and Local homogeneity Transformation, we use the sketch image as a homogenous image to perform the corresponding transformation in sketch re-identification. The transformation results are shown in Fig.10.

[31] proposed a joint feature learning architecture to simultaneously learn individual distinguishing features and domain invariant features. Sketch and pedestrian photos are extracted by pedestrian sketch feature generator and pedestrian photo feature generator respectively, and the extracted features are identified by pedestrian ID confirmation sub network and domain discriminator sub network respectively. Among them, the pedestrian ID confirmation sub network represents the individual feature learning task, which can be the pedestrian ID classification and confirmation task, and is used to learn individual distinguishing features. The domain discriminator is introduced to set up the task of antagonism feature learning. The optimization goal of the domain discriminator is to distinguish whether the input feature is from sketch or pedestrian image as far as possible. The optimization goal of the feature generator is to generate domain invariant features as far as possible. Therefore, the optimization goal of the two feature generators and the domain discriminator is antagonism. In fact, the feature generator and the domain discriminator are optimized alternately. Obviously, this method is cumbersome and complicated.

In order to make a fair comparison, as same as [31], the method proposed in this paper is firstly trained on the market-1501 dataset, and then fine tuned on sketch ReID dataset. In parameter setting, this paper set 5% Global Sketch Transformation and 70% Local Sketch Transformation.

**Table 4.** Performance comparison on sketch ReID dataset.

sketch ReID dataset	Rank-1	Rank-5	Rank-10
Adversarial Feature Learning[31]	34.0%	56.3%	72.5%
GST+LST(ours)	42.5%	70.0%	87.5%

The experiment result shows that the performance improvement in the Sketch Re-identification more than 8%. This experiment also shows the generality of the proposed method.

## 6 Conclusion

In this paper, a simple, effective and general multi-modal data learning method is proposed. Neither does the method require large scale training like GAN, nor introduces any noise. In addition, it can increase the diversity of training samples. At the same time, the method uses a random homogeneous transformation to realize the modeling of different modal relationships. Experiments on several datasets and benchmark show that the proposed method is effective and outperforms the current optimal algorithm.

## References

1. Hao Luo, Youzhi Gu, Xingyu Liao, Shenqi Lai, Wei Jiang; Bag of Tricks and A Strong Baseline for Deep Person Re-identification. In the IEEE Conference on Computer Vision and Pattern Recognition (CVPR) Workshops, 2019.
2. Lingxiao He, Xingyu Liao, Wu Liu, Xinchen Liu, Peng Cheng, Tao Mei; FastReID: A Pytorch Toolbox for General Instance Re-identification arXiv preprint arXiv :2006.02631,2020.
3. Zhun Zhong, Liang Zheng, Guoliang Kang, Shaozi Li, and Yi Yang. Random erasing data augmentation. arXiv preprint arXiv:1708.04896, 2017.
4. Yifan Sun, Changmao Cheng, Yuhan Zhang, Chi Zhang, Liang Zheng, Zhongdao Wang, Yichen Wei; Circle loss:A unified perspective of pair similarity optimization.The IEEE/CVF Conference on Computer Vision and Pattern Recognition (CVPR), 2020.
5. Xing Fan, Wei Jiang, Hao Luo, and Mengjuan Fei. SphereReID: Deep hypersphere manifold embedding for person re-identification. Journal of Visual Communication and Image Representation, 2019.
6. Christian Szegedy, Vincent Vanhoucke, Sergey Ioffe, JonShlens,and ZbigniewWojna. Rethinking the inception architecture for computer vision. In Proceedings of the IEEE conference on computer vision and pattern recognition, pages 2818–2826, 2016.

7. Zhun Zhong, Liang Zheng, Donglin Cao, and Shaozi Li. Re-ranking person re-identification with k-reciprocal encoding. In The IEEE Conference on Computer Vision and Pattern Recognition (CVPR), 2017.
8. Zheng, Zhedong and Yang, Xiaodong and Yu, Zhiding and Zheng, Liang and Yang, Yi and Kautz, Jan; Joint Discriminative and Generative Learning for Person Re-identification. In the IEEE Conference on Computer Vision and Pattern Recognition (CVPR) 2019.
9. Kaiyang Zhou, Yongxin Yang, Andrea Cavallaro, and Tao Xiang. Omni-scale feature learning for person re-identification. In The IEEE International Conference on Computer Vision (ICCV), 2019.
10. [https://github.com/layumi/ReID\\_baseline\\_pytorch](https://github.com/layumi/ReID_baseline_pytorch)
11. P. Fang, J. Zhou, S. K. Roy, L. Petersson, and M. Harandi. Bilinear attention networks for person retrieval. In The IEEE International Conference on Computer Vision (ICCV), 2019, pp. 8030–8039.
12. M. Ye, J. Shen and L. Shao, Visible-Infrared Person Re-Identification via Homogeneous Augmented Tri-Modal Learning, in IEEE Transactions on Information Forensics and Security, doi: 10.1109/TIFS.2020.3001665.
13. Liang Zheng, Liyue Shen, Lu Tian, Shengjin Wang, Jing-dong Wang, and Qi Tian. Scalable person re-identification: A benchmark. In ICCV, 2015.
14. Z. Zheng, L. Zheng, and Y. Yang. Unlabeled samples generated by gan improve the person re-identification baseline in vitro. In ICCV, 2017.
15. Yifan Sun, Changmao Cheng, Yuhan Zhang, Chi Zhang, Liang Zheng, Zhongdao Wang, and Yichen Wei. Circle loss: A unified perspective of pair similarity optimization. In the IEEE Conference on Computer Vision and Pattern Recognition (CVPR), 2020.
16. Longhui Wei, Shiliang Zhang, Wen Gao, Qi Tian; Person Transfer GAN to Bridge Domain Gap for Person Re-Identification Proceedings of the IEEE Conference on Computer Vision and Pattern Recognition (CVPR), 2018.
17. Xingyang Ni, Liang Fang, Heikki Huttunen. AdaptiveReID: Adaptive L2 Regularization in Person Re-Identification. arXiv preprint arXiv :2007.07875, 2020.
18. X. Chen, C. Fu, Y. Zhao, F. Zheng, J. Song, R. Ji, and Y. Yang. Saliency-Guided Cascaded Suppression Network for Person Re-Identification. In The IEEE Conference on Computer Vision and Pattern Recognition (CVPR), 2020.
19. Z. Zhang, C. Lan, W. Zeng, X. Jin, and Z. Chen. Relation-Aware Global Attention for Person Re-identification. In The IEEE Conference on Computer Vision and Pattern Recognition (CVPR), 2020.
20. Yifan Sun, Liang Zheng, Yi Yang, Qi Tian, and Shengjin Wang. Beyond part models: Person retrieval with refined part pooling (and a strong convolutional baseline). In The European Conference on Computer Vision (ECCV), 2018.
21. Kaiyang Zhou, Yongxin Yang, Andrea Cavallaro, and Tao Xiang. Omni-scale feature learning for person re-identification. In The IEEE International Conference on Computer Vision (ICCV), 2019.
22. Bryan (Ning) Xia, Yuan Gong, Yizhe Zhang, and Christian Poellabauer. Second-order non-local attention networks for person re-identification. In The IEEE International Conference on Computer Vision (ICCV), 2019.
23. Binghui Chen, Weihong Deng, and Jiani Hu. Mixed highorder attention network for person re-identification. In The IEEE International Conference on Computer Vision (ICCV), 2019.
24. Chiat-Pin Tay, Sharmili Roy, and Kim-Hui Yap. Aanet: Attribute attention network for person re-identifications. In The IEEE Conference on Computer Vision and Pattern Recognition (CVPR), 2019.

25. Ruibing Hou, Bingpeng Ma, Hong Chang, Xinqian Gu, Shiguang Shan, and Xilin Chen. Interaction-and-aggregation network for person re-identification. In The IEEE Conference on Computer Vision and Pattern Recognition (CVPR), 2019.
26. Feng Zheng, Cheng Deng, Xing Sun, Xinyang Jiang, Xiaowei Guo, Zongqiao Yu, Feiyue Huang, and Rongrong Ji. Pyramidal person re-identification via multi-loss dynamic training. In The IEEE Conference on Computer Vision and Pattern Recognition (CVPR), 2019.
27. Binghui Chen, Weihong Deng, and Jiani Hu. Mixed highorder attention network for person re-identification. In The IEEE International Conference on Computer Vision (ICCV), 2019.
28. Ruijie Quan, Xuanyi Dong, Yu Wu, Linchao Zhu, and Yi Yang. Auto-ReID: Searching for a part-aware convnet for person re-identification. In The IEEE International Conference on Computer Vision (ICCV), 2019.
29. Mang Ye, Jianbing Shen, Gaojie Lin, Tao Xiang, Ling Shao, Steven C. H. Hoi. Deep Learning for Person Re-identification: A Survey and Outlook[J]. In IEEE transactions on pattern analysis and machine intelligence (TPAMI), 2021.
30. Mang Ye, Xiangyuan Lan, Jiawei Li, Pong C. Yuen: Hierarchical Discriminative Learning for Visible Thermal Person Re-Identification. AAAI 2018: 7501-7508
31. Lu Pang, Yaowei Wang, Yi-Zhe Song, Tiejun Huang, Yonghong Tian; Cross-Domain Adversarial Feature Learning for Sketch Re-identification; ACM Multimedia 2018